

Probing attosecond pulse structures by XUV-induced hole dynamics

Jih-An You,^{1,2} Nina Rohringer,^{1,2} and Jan Marcus Dahlström^{1,2,3}

¹Max Planck Institute for the Physics of Complex Systems, Noethnitzerstr. 38, 01187 Dresden

²Center for Free-Electron Laser Science, Luruper Chaussee 149, 22761 Hamburg*

³Department of Physics, Stockholm University, AlbaNova University Center, SE-106 91 Stockholm†

We investigate a two-photon ionization process in neon by an isolated attosecond pump pulse and two coherent extreme ultraviolet probe fields. The probe fields, tuned to the 2s–2p transition in the residual ion, allow for coherent control of the photoelectron via indirect interactions with the hole. We show that the photoelectron–ion coincidence signal contains an interference pattern that can be used to reconstruct the temporal structure of attosecond pump pulses. Our results are supported by simulations based on time-dependent configuration–interaction singles and lowest-order perturbation theory within second quantization.

Atoms and molecules are today routinely probed and controlled on the atomic time scale (1 a.u. = 24.2 as = 24.2×10^{-18} s) in various branches of attophysics [1]. Tailored laser fields allow for control of electron trajectories [2, 3] and for probing the generation of attosecond pulses [4, 5]. Attosecond XUV-pump – IR-probe experiments allow for studies of hole dynamics in molecules [6] and for direct control of autoionization processes in the time domain [7]. Conversely, real-time hole dynamics in atoms can be initiated by an intense IR-pump and then probed by an isolated attosecond pulse [8]. However, one long standing goal of attosecond science, that is to provide an exact temporal characterization tool for isolated attosecond pulses, has so far been inconvenienced by the delayed response in photoemission [9]. Attosecond pulses have mainly been characterized using streak-camera techniques [10–12], or interferometric techniques [13–15], where photoelectrons are treated as “replicas” of the corresponding attosecond pulses. The sought-after group delay of the pulses is then extracted after manipulation of the replicas by a phase-locked infrared (IR) laser field. Recent difference measurements have evidenced that such XUV–IR schemes, which rely on laser-driven photoelectron dynamics, suffer from errors on the order of tens of attoseconds [9], or more [16]. These delays, or “response times”, have stimulated further theoretical investigations, where it was shown that the IR field couples with the ionic potential and distorts the signal from the photoelectron replica of the attosecond pulse [17–20].

In this letter, we investigate interference of two-photon XUV absorption processes by an isolated attosecond pulse and a pair of narrowband XUV probe fields in neon. The coherent probe fields are tuned to stimulate hole transitions in the ion, rather than the usual electron continuum dynamics. A small red and blue detuning of the probe fields relative to the resonant hole transition is used to induce spectral shearing of the photoelectron replica

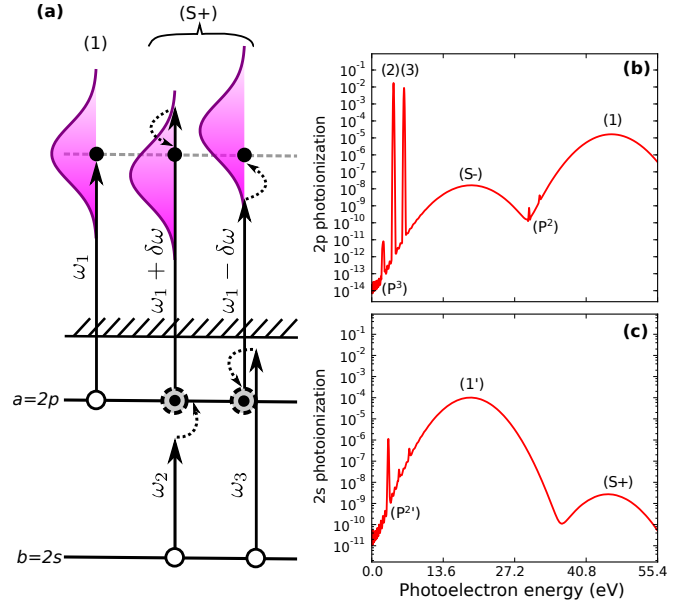


FIG. 1. (Color online) (a) Photoionization processes in neon: (1) attosecond pulse photoelectron replica by one-photon from outer valence $a = 2p$; and (S+) non-sequential two-photon processes generating spectrally sheared replicas by stimulated ionic transitions leading to with a final hole in the inner valence $b = 2s$. (b) Outer-valence photoelectron spectrum. (c) Inner-valence photoelectron spectrum. See main text for the labeled spectroscopic structures.

to lower and higher kinetic energies, respectively. The shearing process is illustrated under (S+) in Fig. 1 (a) relative to (1), the unshifted one-photon ionization process. This opens up for a novel control scheme of the final electron energy by *indirect* interaction with the probe fields via the hole in the remaining ion. Interestingly, we also show that direct interactions between the electron and the hole are not required to explain the mechanism and that the process is well described by either time-dependent simulations or perturbation theory within the independent particle approximation.

We consider the total spectral XUV amplitude of the

* Present address: Max Planck Institute for the Structure and Dynamics of Matter, Luruper Chaussee 149, 22761 Hamburg

† marcus.dahlstrom@fysik.su.se

incoming field (for positive frequencies) on the neon atom to be

$$E(\omega) = E_1(\omega) + E_2\delta(\omega - \omega_2) + E_3\delta(\omega - \omega_3), \quad (1)$$

where the pump amplitude is $E_1(\omega) = |E_1(\omega)|\exp[i\phi_1(\omega)]$ with a central energy, ω_1 and a spectral bandwidth, $\Delta\omega_1$. The group delay, $\tau_1^{(\text{GD})} = d\phi_1/d\omega$, describes the arrival time of a particular frequency component ω , on the target neon atom. Further, we consider probe frequencies that are symmetrically red and blue shifted relative to a given hole transition from the outer valence state, $a = 2p$ with energy $\epsilon_a = -21.56$ eV, to the inner valence state, $b = 2s$ with energy $\epsilon_b = -48.47$ eV, in neon [21] (atomic units: $\hbar = e = m = 4\pi\epsilon_0 = 1$ are used unless otherwise stated)

$$\begin{aligned} \omega_2 &= \epsilon_a - \epsilon_b - \delta\omega \\ \omega_3 &= \epsilon_a - \epsilon_b + \delta\omega, \end{aligned}$$

where the detuning is small compared to the bandwidth of the pump field, $\delta\omega \ll \Delta\omega_1$. In Eq. (1) we assumed that the probe fields are monochromatic but in practice it is sufficient that the bandwidth is much smaller than the detuning, $\Delta\omega_{2,3} \ll \delta\omega$. The group delay of the probe fields is defined as $\tau_{3,2}^{(\text{GD})} = (\phi_3 - \phi_2)/2\delta\omega$ using the spectral phase of the probe fields, $\phi_{2,3} = \arg\{E_{2,3}\}$. Because of interference between the two probe paths, the photoelectron-hole coincidence signal W_{pb} , for the non-sequential pump-probe processes is modulated with the relative group delay of pump and probe fields. Within perturbation theory W_{pb} has the following structure

$$W_{pb} = |A_{pb}| - |B_{pb}| \cos \left[2\delta\omega \left(\tau_1^{(\text{GD})} - \tau_{3,2}^{(\text{GD})} + \tau_{pb} \right) \right], \quad (2)$$

where pb labels the final state of photoelectron ϕ_p and the hole in the atom ϕ_b . In Eq. (2), $|A_{pb}|$ is the incoherent sum of the transition strengths, while $|B_{pb}|$ relates to the cross term of the amplitudes, both are independent of the delay of the fields. If the response time, τ_{pb} in Eq. (2), is negligible, or known, then the desired $\tau_1^{(\text{GD})}$ can be directly reconstructed by measuring the W_{pb} signal as a function of $\tau_{3,2}^{(\text{GD})}$. The fact that W_{pb} depends on both the state of the electron and the hole (ion) implies that an advanced coincidence detection scheme must be used to realize the technique, e.g. by a reaction microscope [22] or by fluorescence detection [23]. Recent advances in attophysics already include both electron-ion [24] and electron-electron coincidence measurements [25].

In Fig. 1 (c) and (d) we show simulated ionic channel resolved photoelectron spectra for a one-dimensional model of the neon atom. The numerical method is based on time-dependent configuration-interaction singles (TDCIS) [26] with a coupled surface flux method [27]. Recently, a similar implementation was used by Karamatskou *et al.* [28]. We have extended this framework, by allowing for redistribution of channel populations due to hole dynamics after the electron has escaped

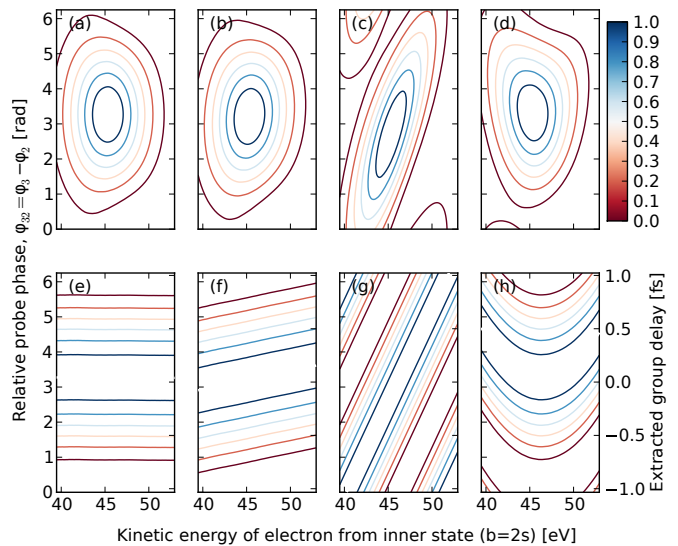


FIG. 2. (a)–(d) (Color online) Normalized photoelectron distribution of the (S+) peak in Fig. 1 (c), as a function of the phase difference between probe fields. (a) Fourier limited pump pulse; (b,c) linear chirp; and (d) quadratic chirp of pump pulse. (e)–(h) same as (a)–(d) but with normalization at each individual kinetic energy. The dashed white curve shows the extracted sub-femtosecond group delay of the pump pulse.

the inner region. Here, we consider an independent-particle model, with an effective potential that matches the ionization energies of neon, but we have also performed simulations including electron-electron interactions and found qualitatively identical results. Further details about the numerical method are given in the supplemental material.

Photoelectrons leaving the residual ion with a hole in the $2p$ state [Fig. 1 (c)] exhibit one broad peak (1) due to absorption of one pump photon (with a central photon energy chosen as $\omega_1 = 68$ eV and $\Delta\omega_1 = 7.5$ eV) and two narrow peaks (2,3) due to absorption of either probe field (with photon energies chosen as $\omega_{2,3} = 26.9 \mp 1$ eV with $\Delta\omega_{2,3} = 0.125$ eV). The broad peak (S-) is due to absorption of one pump photon and stimulated emission of a probe photon. Weaker peaks labeled with (P²) and (P³) denote two and three probe-photon processes, respectively. Photoelectrons leaving the residual ion with a hole in the $2s$ -state [Fig. 1 (d)] exhibit a peak (1') from the pump field and a peak (S+) due to absorption of one pump and one probe photon.

In Fig. 2, we show the detailed behaviour of the (S+) structure as a function of relative probe phase, $\phi_{32} = \phi_3 - \phi_2$, for (a) a Fourier limited pump pulse, $\phi_1(\omega) = 0$; (b,c) a quadratic phase dependence, $\phi_1(\omega) = \alpha(\omega - \omega_1)^2$ with $\alpha = 10$ and 100 , respectively; and (d) a cubic phase dependence, $\phi_1(\omega) = \beta(\omega - \omega_1)^3$ with $\beta = 100$. For a fourier-limited attosecond pulse [Fig. 2 (a)], the (S+) peak vanishes at synchronized probe fields, $\phi_{32} \approx 0$; while the peak is maximized for $\phi_{32} \approx \pi$. This is due to in-

interference between the two probe paths that transition through different sides of the hole resonance and, therefore, carry a relative π -shift. In Fig. 2 (e)–(h) we verify the delay-dependent modulation of Eq. (2), by dividing every phase-dependent curve, at a fixed energy of Fig. 2. (a)–(d), by its maximal value. The extracted group-delays (white dashed curves) show the expected (e) constant value (b,c) linear chirp and (d) quadratic chirp, with good recovery of the phase parameters, indicating that the response time of the system, τ_{pb} in Eq. (2), is small. Our extracted (actual) phase parameters are $\alpha = 0.01$ (0), 9.95 (10), 99.4 (100) and $\beta = 99.1$ (100), for the four pump pulses, respectively, with an estimated error of ± 0.2 based on variation of the energy range in the fitting. As mentioned, we have additionally performed simulations using a correlated TDCIS model, including electron–electron interactions, and we find qualitatively the same result. This shows that correlation effects are not required to explain the indirect control of the photoelectron by the probe field that act predominately (or even exclusively) on the hole in the ion.

In Fig. 3 (a) we show the response time τ_{pb} , of neon using a more realistic, three-dimensional model based on an independent-particle approximation. The complex amplitude for two-photon ionization by first absorption of a photon ω'_1 , from the broad-band XUV pump field $E_1(\omega'_1)$, followed by absorption of a second photon ω_f , by a monochromatic probe field E_f , is given by

$$S_{pb} = \frac{1}{2\pi i} E_f E_1(\omega_{pb} - \omega_f) M_{pb}(\omega_{pb} - \omega_f, \omega_f), \quad (3)$$

where pb labels the state of the final electron ϕ_p , with energy $\epsilon_p > 0$, and the final hole in the atom ϕ_b , with energy $\epsilon_b < 0$. It is assumed that the excitation starts from the atomic ground state and that the final hole is in the inner valence state, $b = 2s$. In writing Eq. (3) we have imposed energy conservation for the total process, $\epsilon_p - \epsilon_b \equiv \omega_{pb} = \omega'_1 + \omega_f$. The two-photon matrix element in Eq. (3) can be separated into two terms using second quantization,

$$M_{pb}(\omega'_1, \omega_f) \approx M_{pb}^{(h)}(\omega'_1, \omega_f) + M_{pb}^{(e)}(\omega'_1, \omega_f), \quad (4)$$

because the probe field can either stimulate a hole transition (h) or an electron transition (e), as illustrated in Fig. 3 (c)–(d). The stimulated hole term,

$$M_{pb}^{(h)}(\omega'_1, \omega_f) = - \sum_{a'} \frac{\langle a' | z | b \rangle \langle p | z | a' \rangle}{(\omega'_1 - \epsilon_p + \epsilon_{a'})} \in \mathbb{R}, \quad (5)$$

describes ejection of an electron from any occupied single-particle state $\phi_{a'}$, to the final electron state ϕ_p , followed by a transition of the hole to the final state ϕ_b . For simplicity, we consider single-particle states that are expanded on a spherical basis, $\phi_i(\mathbf{r}) = R_{n_i, l_i}(r) Y_{l_i, m_i}(\hat{\mathbf{r}})$, with radial wavefunctions, $R_i(r)$, that are eigenstates to the restricted Hartree-Fock equation for occupied states [29]. The unoccupied (virtual) states are additionally

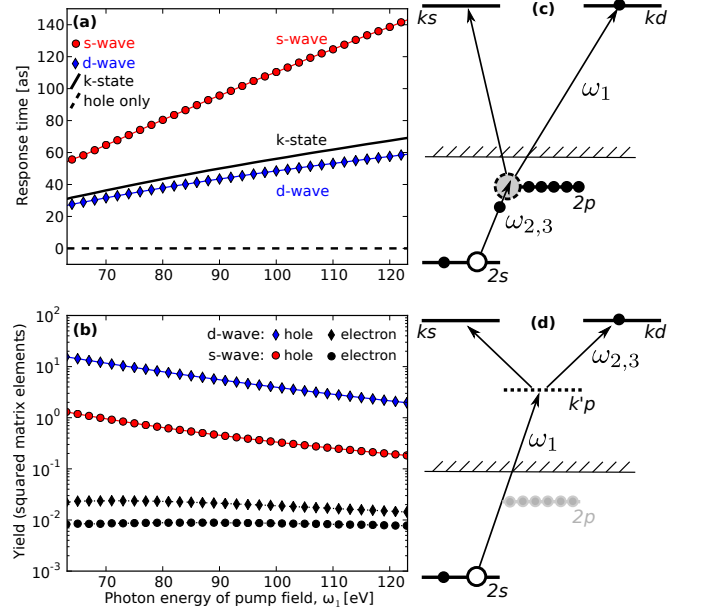


FIG. 3. (a) (Color online) Response time τ_{pb} , for photoelectron ejection along the polarization of the XUV fields $\phi_p = \phi_{\mathbf{k}||\mathbf{z}}$ (black curve); and on the partial d (diamonds) and s (circles) waves, $\phi_p = \phi_{Ed,Es}$. (b) Yield, $|M_{pb}^{(x)}|^2$, for stimulated hole transitions ($x=h$; red and blue symbols) and stimulated electron continuum transitions ($x=e$; black symbols). (c) Two-photon diagram for stimulated hole transition, $2p \rightarrow 2s$, after electron ejection from an outer-valence state, $2p \rightarrow ks/d$. (d) Two-photon diagram for stimulated electron continuum transition from an inner valence state, $2s \rightarrow k'p \rightarrow ks/d$. The probe field detuning in (a) and (b) is $\delta\omega = 1$ eV.

attracted by an effective spherical potential to model the long-range Coulomb interaction between electron and ion, c.f. Ref. [30]. Both initial and final radial orbitals are chosen to be real. If the second photon is in the XUV range it can be tuned close to an ionic transition, $\omega_f \approx \omega_{ab}$, and efficiently stimulate this particular transition in the remaining ion. Under these conditions hole transitions dominate over electron continuum transitions, $|M_{pb}^{(h)}|^2 \gg |M_{pb}^{(e)}|^2$, as shown in Fig. 3 (b) for $\delta\omega = 1$ eV. If $M_{pb}^{(e)}$ is neglected completely, the phase of the spectrally-sheared replica is intact (modulo π) because the matrix element in Eq. (5) is real (for detuned probe fields, $\omega_f \neq \epsilon_{a'} - \epsilon_b$).

The stimulated electron term,

$$\begin{aligned} M_{pb}^{(e)}(\omega'_1, \omega_f) &= \lim_{\xi \rightarrow 0^+} \sum_{p'} \frac{\langle p | z | p' \rangle \langle p' | z | b \rangle}{(\omega'_1 - \epsilon_{p'} + \epsilon_b + i\xi)} \\ &= \text{p.v.} \sum_{p'} \frac{\langle p | z | p' \rangle \langle p' | z | b \rangle}{(\omega'_1 - \epsilon_{p'} + \epsilon_b)} \\ &\quad - \sum_{l_r} i\pi \langle p | z | r \rangle \langle r | z | b \rangle \in \mathbb{C}, \end{aligned} \quad (6)$$

describes an initial dipole interaction that excites an electron from an occupied state ϕ_b , to the unoccupied states,

$\phi_{p'}$. The second dipole interaction then stimulates an electron transition in the continuum to the final state ϕ_p , here, evaluated using the numerical machinery of Ref. [30]. Although the initial and final radial wavefunctions are real functions, the two-photon matrix element in Eq. (6) is a complex quantity. Application of the Sokhotski-Plemelj theorem, on the second line of Eq. (6), leads to real non-resonant contributions (principal-value integrals over p') and imaginary resonant contributions (via intermediate states ϕ_r that are resonant with the first photon, $\epsilon_r = \epsilon_b + \omega'_1$).

The stimulated electron transition is, in general, a good approximation for the total two-photon matrix element, $M_{pb} \approx M_{pb}^{(e)}$, when the probe field is in the IR range. This is because the IR photon does not have enough energy to stimulate ionic transitions in singly ionized noble gas atoms. In the case studied here, with resonant XUV probe fields, the total matrix element is better approximated as a real hole transition plus an imaginary resonant electron transition,

$$M_{pb} \approx M_{pb}^{(h)} + i\text{Im}M_{pb}^{(e)}. \quad (7)$$

For small detuning the hole term is dominant so that the total phase, $\arg(M_{pb})$, is close to 0 or π radians with a small correction given by the resonant electron term. The total signal, Eq. (2), can now be analyzed by absolute square of the summed complex amplitudes of probe fields $f = 2, 3$ given in Eq. (3). For simplicity, we assume that the resonant electron term is independent of the detuning, so that the response time can be approximated as

$$\tau_{pb} \approx \frac{1}{\delta\omega} \arctan \left[\frac{\pi z_{pr} z_{rb}}{z_{ab} z_{pa} \delta\omega} \right] \approx \frac{\pi z_{pr} z_{rb}}{z_{ab} z_{pa}}, \quad (8)$$

where z_{ij} denotes the dipole matrix element between single particle states ϕ_i and ϕ_j . Eq. (8) shows that the response time τ_{pb} is universal and independent of the detuning (provided that the detuning is small, $\delta\omega \ll$

$z_{ab} z_{pa} / \pi z_{pr} z_{rb}$). This robustness to the detuning parameter has also been verified by the TDCIS method described above.

As expected, an ideal instantaneous response ($\tau_{pb} = 0$ at all energies) is found when the model is restricted to stimulated hole transitions, shown by dashed line in Fig. 3 (a). However, when stimulated photoelectron dynamics are included, the response time exhibits a linear drift on both final partial waves, ks and kd , shown by circles and diamonds, respectively in Fig. 3 (a). Similarly, the detection of a photoelectron with momentum along the laser polarization axis exhibits a linear drift of 0.634 as/eV (black line). Over a large energy range, from 65 to 120 eV, the deviation from this linear fit is less than one attosecond. The response time carries information about the relative strength of stimulated hole and electron dynamics, which differ by approximately 2–3 orders of magnitude, as is shown in Fig. 3 (b). The total response time, being on the atomic time scale, establishes the proposed scheme as an all-XUV method for direct group-delay determination.

In conclusion, we have investigated a novel scheme to control the energy of photoelectrons by indirect interaction with a probe field via stimulated hole transitions in the remaining ion. Our work shows that the emerging technologies of attosecond coincidence detection [24, 25] and sub-femtosecond XUV-pump – XUV-probe setups [31] open up for alternative pulse characterization schemes with response times on the atomic time scale. Given the phenomenal interest in attosecond photoionization response time measurements spurred by Ref. [9], we expect our method is a welcome addition for cross-check measurements of isolated attosecond pulses.

ACKNOWLEDGMENTS

J.M.D. acknowledges financial support from the Swedish Research Council (VR).

-
- [1] Ferenc Krausz and Misha Ivanov. Attosecond physics. *Rev. Mod. Phys.*, 81:163–234, Feb 2009.
 - [2] P. Eckle, A. N. Pfeiffer, C. Cirelli, A. Staudte, R. Dörner, H. G. Muller, M. Büttiker, and U. Keller. Attosecond ionization and tunneling delay time measurements in helium. *Science*, 322:1525–1529, 2008.
 - [3] S. Haessler, T. Balčiunas, G. Fan, G. Andriukaitis, A. Pugžlys, A. Baltuška, T. Witting, R. Squibb, A. Zaïr, J.W.G. Tisch, J.P. Marangos, and L.E. Chipperfield. Optimization of quantum trajectories driven by strong-field waveforms. *Phys. Rev. X*, 4:021028, 2014.
 - [4] Dror Shafir, Hadas Soifer, Barry D. Bruner, Michal Dagan, Yann Mairesse, Serguei Patchkovskii, Misha Yu. Ivanov, Olga Smirnova, and Nirit Dudovich. Resolving the time when an electron exits a tunnelling barrier. *Nature*, 485:343–346, May 2012.
 - [5] Kyung Taec Kim, Chunmei Zhang, Andrew D. Shiner, Sean E. Kirkwood, Eugene Frumker, Genevieve Gariepy, Andrei Naumov, D. M. Villeneuve, and P. B. Corkum. Manipulation of quantum paths for space-time characterization of attosecond pulses. *Nature Physics*, 9:159–163, 2013.
 - [6] F. Calegari, D. Ayuso, A. Trabattori, L. Belshaw, S. De Camillis, S. Anumula, F. Frassetto, L. Poletto, A. Palacios, P. Decleva, J. B. Greenwood, F. Martín, and M. Nisoli. Ultrafast electron dynamics in phenylalanine initiated by attosecond pulses. *Science*, 346:336–339, 2014.
 - [7] Christian Ott, Andreas Kaldun, Philipp Raith, Kristina Meyer, Martin Laux, Jörg Evers, Christoph H. Keitel, Chris H. Greene, and Thomas Pfeifer. Lorentz meets fano in spectral line shapes: A universal phase and its

- laser control. *Science*, 340:716–720, 2013.
- [8] Eleftherios Goulielmakis, Zhi-Heng Loh, Adrian Wirth, Robin Santra, Nina Rohringer, Vladislav S. Yakovlev, Sergey Zherebtsov, Thomas Pfeifer, Abdallah M. Azzeer, Matthias F. Kling, Stephen R. Leone, and Ferenc Krausz. Real-time observation of valence electron motion. *Nature*, 466:739–743, 2010.
- [9] M. Schultze, M. Fiess, N. Karpowicz, J. Gagnon, M. Korbman, M. Hofstetter, S. Neppl, A. L. Cavalieri, Y. Komninos, Th. Mercouris, C. A. Nicolaides, R. Pazourek, S. Nagele, J. Feist, J. Burgdörfer, A. M. Azzeer, R. Ernstorfer, R. Kienberger, U. Kleineberg, E. Goulielmakis, F. Krausz, and V. S. Yakovlev. Delay in photoemission. *Science*, 328:1658–1662, 2010.
- [10] M. Hentschel, R. Kienberger, Ch. Spielmann, G. A. Reider, N. Milosevic, T. Brabec, P. Corkum, U. Heinzmann, M. Drescher, and F. Krausz. Attosecond metrology. *Nature*, 414:509 – 513, 2001.
- [11] J. Itatani, F. Quéré, G. L. Yudin, M. Yu. Ivanov, F. Krausz, and P. B. Corkum. Attosecond streak camera. *Phys. Rev. Lett.*, 88:173903, 2002.
- [12] R. Kienberger, E. Goulielmakis, M. Uiberacker, A. Baltuska, V. Yakovlev, F. Bammer, A. Scrinzi, Th. Westerwalbesloh, U. Kleineberg, U. Heinzmann, M. Drescher, and F. Krausz. Atomic transient recorder. *Nature*, 427:817 – 821, 2004.
- [13] P. M. Paul, E. S. Toma, P. Breger, G. Mullot, F. Augé, Ph. Balcou, H. G. Muller, and P. Agostini. Observation of a train of attosecond pulses from high harmonic generation. *Science*, 292(5522):1689–1692, 2001.
- [14] Michael Chini, Steve Gilbertson, Sabih D. Khan, and Zenghu Chang. Characterizing ultrabroadband attosecond lasers. *Opt. Express*, 18:13006–13016, 2010.
- [15] Michael Chini, Kun Zhao, and Zenghu Chang. The generation, characterization and applications of broadband isolated attosecond pulses. *Nature Photonics*, 8:178–186, 2014.
- [16] K. Klünder, J. M. Dahlström, M. Gisselbrecht, T. Fordell, M. Swoboda, D. Guénot, P. Johnsson, J. Caillat, J. Mauritsson, A. Maquet, R. Taïeb, and A. L’Huillier. Probing single-photon ionization on the attosecond time scale. *Phys. Rev. Lett.*, 106:143002, 2011.
- [17] C.-H. Zhang and U. Thumm. Electron-ion interaction effects in attosecond time-resolved photoelectron spectra. *Phys. Rev. A*, 82:043405, 2010.
- [18] S. Nagele, R. Pazourek, J. Feist, K. Doblhoff-Dier, C. Lemell, K. Tókési, and J. Burgdörfer. Time-resolved photoemission by attosecond streaking: extraction of time information. *Journal of Physics B: Atomic, Molecular and Optical Physics*, 44:081001, 2011.
- [19] Misha Ivanov and Olga Smirnova. How accurate is the attosecond streak camera? *Phys. Rev. Lett.*, 107:213605, 2011.
- [20] J M Dahlström, A L’Huillier, and A Maquet. Introduction to attosecond delays in photoionization. *Journal of Physics B: Atomic, Molecular and Optical Physics*, 45:183001, 2012.
- [21] A. Kramida, Yu. Ralchenko, J. Reader, and NIST ASD Team. NIST Atomic Spectra Database (ver. 5.2), [Online]. Available: <http://physics.nist.gov/asd> [2015, June 30]. National Institute of Standards and Technology, Gaithersburg, MD., 2014.
- [22] Joachim Ullrich, Robert Moshhammer, Alexander Dorn, Reinhard Dörner, L. Ph. H. Schmidt, and H. Schmidt-Böcking. Recoil-ion and electron momentum spectroscopy: reaction-microscopes. *Rep. Prog. Phys.*, 66:1463, 2003.
- [23] J.-E. Rubensson, J. Lüning, M. Neeb, B. Küpper, S. Eisebitt, and W. Eberhardt. Photoelectron soft x-ray fluorescence coincidence spectroscopy on free molecules. *Phys. Rev. Lett.*, 76:3919–3922, May 1996.
- [24] M. Sabbar, S. Heuser, R. Boge, M. Lucchini, L. Gallmann, C. Cirelli, and U. Keller. Combining attosecond xuv pulses with coincidence spectroscopy. *Review of Scientific Instruments*, 85:103113, 2014.
- [25] Erik P. Mansson, Diego Guenet, Cord L. Arnold, David Kroon, Susan Kasper, J. Marcus Dahlström, Eva Lindroth, Anatoli S. Kheifets, Anne L’Huillier, Stacey L. Sorensen, and Mathieu Gisselbrecht. Double ionization probed on the attosecond timescale. *Nature Physics*, 10:207 – 211, 2014.
- [26] Nina Rohringer, Ariel Gordon, and Robin Santra. Configuration-interaction-based time-dependent orbital approach for *ab initio* treatment of electronic dynamics in a strong optical laser field. *Phys. Rev. A*, 74:043420, 2006.
- [27] Liang Tao and Armin Scrinzi. Photo-electron momentum spectra from minimal volumes: the time-dependent surface flux method. *New Journal of Physics*, 14:013021, 2012.
- [28] Antonia Karamatskou, Stefan Pabst, Yi-Jen Chen, and Robin Santra. Calculation of photoelectron spectra within the time-dependent configuration-interaction singles scheme. *Phys. Rev. A*, 89:033415, Mar 2014.
- [29] I. Lindgren and J. Morrison. *Atomic Many-Body Theory*. Series on Atoms and Plasmas. Springer-Verlag, New York Berlin Heidelberg, second edition, 1986.
- [30] J M Dahlström and E Lindroth. Study of attosecond delays using perturbation diagrams and exterior complex scaling. *Journal of Physics B: Atomic, Molecular and Optical Physics*, 47:124012, 2014.
- [31] P. Tzallas, E. Skantzakis, L. A. A. Nikolopoulos, G. D. Tsakiris, and D. Charalambidis. Extreme-ultraviolet pump-probe studies of one-femtosecond-scale electron dynamics. *Nature Physics (London)*, 7:781, 2011.